Articles NanoLab

Controlling the Optical Properties of a Conjugated Co-polymer through Variation of Backbone Isomerism and the Introduction of Carbon Nanotubes

A. Dalton
Technological University Dublin

J. Coleman
Trinity College Dublin

M. in Het Panhuis
Trinity College Dublin

B. McCarthy
Trinity College Dublin

A. Drury
Trinity College Dublin

Follow this and additional works at: https://arrow.tudublin.ie/nanolart

Part of the Physics Commons

See next page for additional authors

Authors

A. Dalton, J. Coleman, M. in Het Panhuis, B. McCarthy, A. Drury, W. Blau, J. Nunzi, and Hugh Byrne

Controlling the optical properties of a conjugated co-polymer through variation of backbone isomerism and the introduction of carbon nanotubes

A.B. Dalton[1], J.N. Coleman[2], M. in het Panhuis[2], B. McCarthy[2], A. Drury[2], W.J. Blau[2], B. Paci[3], J. -M. Nunzi[3], H.J. Byrne[1]

[1] Facility for Optical Characterisation and Spectroscopy (FOCAS)/School of Physics, Dublin Institute of Technology, Kevin Street, Dublin 8, Ireland

[2] Materials Ireland Polymer Research Centre, Physics Department, Trinity College Dublin, Dublin 2, Ireland

[3] LETI (CEA-Technologies Avancees) Dein-SPE, Groupe Composants Organiques, Saclay, F 91191 Gif-sur-Yvette, France

Abstract

The need to control the formation of weakly emitting species in polymers such as aggregates and excimers, which are normally detrimental to device performance, is illustrated for the example of the polymer poly(*m*-phenylenevinylene-co-2,5-dioctyloxy-*p*-phenylenevinylene), using the model compound, 2,5-dioctyloxy-*p*-distyrylbenzene as a comparison. Two different methods, namely a Horner-Emmons polycondensation in dimethylformamide (DMF) and a Wittig polycondensation in dry toluene, have been used during synthesis resulting in a polymer with a predominantly *trans*-vinylene backbone and a polymer with a predominantly *cis*-vinylene backbone respectively. Photoluminescence and absorption spectroscopy indicate that the polymer forms aggregate species in solution with spectra that are distinctly red-shifted from those associated with the intra-chain exciton. Concentration dependent optical

studies were used to probe the evolution of aggregation in solution for both polymers. The results indicate that inter-chain coupling in the predominantly *cis* polymer is prominent at lower concentrations than in the case of the *trans* counterpart. These results are supported by pico-second pump and probe transient absorption measurements where, in dilute solutions, the polymer in a *cis*-configuration exhibits highly complex excited state dynamics whereas the polymer in a *trans*-configuration behaves similarly to the model compound. It is proposed therefore that the degree of backbone isomerism has a profound impact on the morphology of the polymeric solid and control over it is a route towards optimising the performance of the material in thin film form. Another method to inhibit inter-chain effects using multi walled carbon nanotubes (MWNT) as nano-spacers in the polymer solutions is proposed. By comparison to spectroscopic analysis, aggregation effects are shown to be reduced by the introduction of nanotubes. Electron microscopy and computer simulation suggest a well-defined interaction between the polymer backbone and the lattice of the nanotube.

1. Introduction

Poly(*p*-phenylenevinylene) (PPV) and its derivatives have been widely studied due to their potential as active materials in light emitting diodes[1,2]. In order for this potential to be realised, a number of problems must be overcome. Two of the major issues are control of emission colour and improvement in emission efficiency. By incorporating appropriate substituents, PPV-derivatives can emit light in the green[3] to red[4] range. However, due to the long conjugation length, it is not normally possible to achieve blue luminescence from this type of material. Recently a number

of methods have been proposed to achieve this end, involving the incorporation of *meta*/*ortho* phenylene units in the PPV backbone[5,6]. These methods have proven successful in interrupting conjugation and thus shifting the emission to higher energies.

The problem of low emission efficiencies is also of critical concern. While materials can be engineered and their properties tailored, molecules or polymer chains are in close proximity to each other in the solid, leading to the possibility of electronic interactions between neighbouring molecules or strands. Such interactions facilitate the formation of weakly emitting species such as aggregates and excimers. The electronic and optical properties of the material deviate substantially from that of the individual molecules, resulting in device performance below that which might be expected. A number of methods have been proposed to inhibit inter-molecular interactions such as the incorporation of bulky side-chains[7] or bridged chain substitution[8]. While these methods have achieved some success, increases in luminescence are often accompanied by a marked loss in charge transport in devices[9]. Another method that has proved successful is the incorporation of *cis* linkages into the backbone[10]. For PPV based light emitting diodes (LED), the result is an enhancement of luminescence as well as a markedly increased current density. Controlling the frequency and distribution of *cis*/*trans* linkages and the effects on the optical properties have been extensively studied in many of the poly(arylenes)[11]. Various polymer-processing approaches have also been reported such as the utilisation of polymer blends[12]. This method involves using a non-conjugated, non-interacting polymer as a spacer to isolate individual molecules or strands.

In this study, poly(*m*-phenylenevinylene-co-2,5-dioctyloxy-*p*-phenylene-vinylene) (PmPV-co-DOctOPV)[1] is employed to illustrate some of these problems and to indicate potential routes towards alleviating them. The alternate *meta*-phenylene linkage leads to a reduction of the conjugation along the backbone. Previously, it was shown that the change in backbone configuration blue shifts the absorption and luminescence as expected[13-14]. It may also be expected that the geometry of the backbone reduce the distances over which phonons can propagate. Consequently, relaxation processes are less likely to be non-radiative. Although it has been shown that 1,3-distyrlbenzene is less fluorescent than 1,4-distyrylbenzene[15], this can be attributed to the different nature of the lowest energy transition, whereas the effect on an extended alternating system has yet to be elucidated.

In the present study, the polymer has been prepared by two different poly-condensation reactions and the optical properties compared. The results indicate that while both samples have the same nominal chemical structure, the optical properties can vary greatly. It is concluded that the differing optical properties result from differing propensities to aggregate in solution and infrared studies indicate that this is due to differing distributions and ratios of *cis*/*trans* vinylene bonds present in the backbone. Transient absorption measurements by the method of Kerr ellipsometry give further indications that while the excited state photodynamics of a predominantly *trans*-polymer are similar to those of a short chain oligomer, those of the *cis*-rich polymer are far more complex. Control over the backbone isomeric content is therefore suggested as a route towards limiting aggregation in this polymeric system.

---

[1] Sometimes referred to as PmPV

Introduction of nano-spacers in the form of multi walled carbon nanotubes (MWNT) is also discussed as a method of limiting interchain interactions. Carbon nanotubes have stimulated a great deal of interest due to their potential applications in nanotechnology[16-17]. A single walled nanotube (SWNT) can be described as a graphene sheet rolled into a cylindrical shape so that the structure is quasi-one-dimensional with axial symmetry. MWNT are coaxial, concentric assemblies of these graphene cylinders separated by approximately the c plane spacing (0.34nm) of graphite. It will be shown that the effect of incorporating carbon nanotubes into a polymer/toluene solution on the optical properties of PmPV-co-DOctOPV is an effective reduction of concentration and a reversal of detrimental aggregation processes. Computer simulation and electron microscopy is used in an attempt to elucidate the nature of this phenomenon.

2. Controlling Optical Properties: Isomerism

2.1 Materials Preparation and Characterisation

The synthetic route to the polymer for each preparation method and a model oligomer, 2,5-dioctyloxy-*p*-distyrylbenzene (3PV), is given elsewhere[18-19]. The nominal chemical structure of the polymer is shown in Figure 1. PmPV-co-DOctOPV was produced in a Horner-Emmons polycondensation reaction in dry DMF to produce a sample referred to herein as HE-PmPV. A Wittig poly-condensation reaction in dry toluene was also used to produce a polymer referred to herein as W-PmPV. The results of the ^{1}H and ^{13}C nuclear magnetic resonance (NMR) measurements (in

deuterated chloroform) clearly indicate that the polymer structure is as proposed in both cases.

The molecular mass characteristics were analysed using gel permeation chromatography (GPC) (referenced to a narrow molecular weight polystyrene standard). The polydispersivity index (M_w/M_n) was found to be less than two for both methods indicating a narrow molecular weight distribution. By comparing the calculated average chain length, it is also obvious that the Horner-Emmons method leads to longer chain lengths. The use of toluene over DMF seems also to be advantageous in this respect. It must be noted, however, that as polystyrene is used as a standard for the GPC calibration, the actual values measured are polystyrene equivalents. The hydrodynamic volume of PmPV-co-DOctOPV is more rod-like than a polystyrene coil. Therefore, caution must be used in interpreting calculated average degrees of polymerisation (n_{av}). For one of the polymer samples, HE-PmPV, a bimodal mass distribution was observed. The mass profile consists of a broad higher molecular mass (M_w = 6500 – 90500 g/mol) accompanied by a much narrower band (M_w = 3000 g/mol). This latter feature may be due to the presence of macrocyclic oligomers.

2.2 Optical Characterisation

Several concentrations per repeating unit were prepared in toluene solution for each sample. UV-Vis absorption and fluorescence spectra measurement were then carried out on each sample using Shimadzu UV-2101PC and Perkin Elmer LS50B spectrometers respectively.

Figure 2 shows a comparison of the absorption and emission spectra for HE-PmPV (A) and W-PmPV (B) toluene solutions at a concentration of 5 x 10^{-5} M in 1mm cuvettes. Although the material as prepared by the two methods have nominally the same chemical structure, their optical properties, and most notably the emission spectra, are significantly different at this concentration. The absorption spectra are characterised by two absorption bands centred at 330 nm and 400 nm for both samples. For W-PmPV, there is also a red-shifted shoulder with an approximate absorption edge at 480 nm. In the case of 3PV, similar spectra are observed but the peaks are blue-shifted by approximately 10 nm (not shown)[19]. Both polymers show broadband photoluminescence emission in the green/red region with a high-energy vibronic peak at 450 nm. HE-PmPV has a second peak at ~480 nm while W-PmPV has a corresponding feature slightly red-shifted at ~490 nm. The most striking difference between the two spectra is the existence of a strong shoulder on the red side of the spectrum of W-PmPV at ~525nm.

Figure 3 shows the absorption spectra (normalised to concentration) of HE-PmPV for several concentrations in toluene solution. In the dilute solution, the spectrum has peaks at 308 and 370 nm with a broad shoulder centred at 430 nm. As the concentration is increased, the peak at 308 nm shifts to lower energy and decreases in intensity. This red shift saturates at approximately 330 nm at a concentration of 5 x 10^{-5} M. The concentration increase also causes the peak at 370 nm to shift to lower energies and decreases in relative intensity. Accompanying this decrease, there is a new absorption feature appearing at 405 nm, which is

continuously red-shifted as the concentration is increased further. It should also be noted that this new feature decreases in relative intensity with concentration.

In Figure 4, the emission profile for HE-PmPV is shown as a function of concentration is shown. Each spectrum has been normalised for concentration. At low concentration, the profile is a typical vibronic progression, having features at 447 nm and 470 nm and a shoulder at 520 nm. As the concentration increases, the profile appears to red shift and decreases in intensity. The spectral changes may be accounted for by re-absorption by the concentration dependent absorption feature to the red of the absorption spectrum. As the absorption evolves with concentration, it encroaches increasingly on the blue side of the emission spectrum, reducing the observed emission and producing an apparent red-shift. In addition to this phenomenon, there is a new emission feature appearing at 530 nm. The weak fluorescence is additional to absorption effects and must be from a new species. These changes suggest that, through the increase in concentration, interchain species are formed (resulting in new features at 405 nm in the absorption and 530 nm in the emission).

Figure 5 shows the absorption spectra for several concentrations of W-PmPV in toluene solution. Similar to the other polymer sample, there is an intensity decrease as the concentration is increased. However, there do not appear to be any new features evolving at lower energies. The 405 nm feature that evolves with concentration in solutions of HE-PmPV is already present in the dilute solution. This suggests that the extent of inter-chain coupling is much greater in W-PmPV sample and therefore has already formed new species at much lower concentrations. The similarly normalised fluorescence spectra for different concentrations of this sample are shown in Figure 6.

While the spectrum shows similar re-absorption effects with increasing concentration, the new features are already present.

The above results indicate that all polymer samples are aggregating as the concentration is increased. Aggregation is a result of weak inter-chain interactions. In dilute solutions, the individual strands are isolated and these interactions can therefore be neglected. As the concentration is increased and the distances between the polymer chains become smaller, these inter-chain forces become more significant. As a result, polymer coils start to entangle to form loose aggregates. Further increases in concentration result in heavy inter-penetration of strands or the formation of strongly bound aggregates. This has been observed in a range of conjugated polymers[20-21]. It is obvious that the extent of aggregation at lower concentrations is much higher for the case of W-PmPV. These differences suggest that this particular sample conforms differently in solution, thus allowing greater inter-chain interaction at smaller concentrations. It is also clear that this aggregation phenomenon has a detrimental effect on the performance of the material, in terms of photoluminescence quantum yield, at higher concentrations and thus in solid form. The difference in the concentration dependence of the material generated by the two synthetic routes does, however, suggest that the performance of the material may be controlled and optimised. Of critical importance is the identification of the differences between the materials and a parameter, which can be quantified and tuned.

2.3 Vibrational spectroscopy

NMR indicates that the material prepared by the two routes described above is identical in chemical composition, GPC suggesting that the Horner-Emmons route leads to higher molecular weight. However, optical characterisation suggests that the material as prepared through the different routes behave significantly differently as a function of concentration in solution, and thus in solid state. Such a concentration dependence points towards differing molecular packing and polymer morphology. Vibrational spectroscopy, as measured by a Matteson Infinity FTIR absorption spectrometer, gives a clear indication of the source of this difference in behaviour. Figure 7 shows the infrared spectra of HE-PmPV and W-PmPV in the low frequency region. The C-H out of plane vibration of the m-phenylene ring is found at 778 cm^{-1}. The typical absorption of the *trans*-vinylene C-H out-of-plane vibration at 963 cm^{-1} is strong but there is also a feature at 691 cm^{-1} indicative of a *cis*-vinylene unit. The relative heights of these two features can be compared to give a quantitative analysis of the *cis* and/or *trans* content of the sample. The ratio of absorption coefficients of the 963 and 691 cm^{-1} bands can be obtained by comparing the absorbance of the 691 cm^{-1} in a *cis*-rich polymer with that of the 963 cm^{-1} band in a *trans*-rich polymer. The ratio of absorption coefficients (*cis*/*trans*) for a similar system, 3PV, was approximated as 2.05 using NMR and IR analysis[19]. The *cis* contents of the PmPV-co-DOctOPV samples were thus calculated using the equation:

$$cis\ (\%) = 100 \left(\frac{2.05 A_{cis}}{2.05 A_{cis} + A_{trans}} \right)$$

Equation 1

A_{cis} and A_{trans} represent absorbencies of the 691 and 963 cm^{-1} bands in the spectrum of an individual sample respectively. The *cis* content in each sample was thus calculated to be 22% (HE-PmPV) and 71% (W-PmPV) respectively.

Analysis of the vibrational spectrum of the material prepared by the two methods indicates that the *cis*-W-PmPV, predominantly *cis* in character, is that which shows the strongest concentration dependence of the optical properties, whereas the HE-PmPV retains the properties of the isolated molecule more effectively. In the next section, pico-second Kerr ellipsometry is used to probe the excited state properties of the polymer in these two conformations.

2.4 Non-Linear Optical Kerr ellipsometry

Kerr ellipsometry (KE) measurements have been performed at different time delays. The experimental set-up for pico-second Kerr ellipsometry is described in ref. [22]. Non-linear optical Kerr ellipsometry is a pump-probe technique allowing the separation of the real and imaginary part of the photo-induced anisotropy. A frequency tripled Nd^{3+}:YAG laser (355 nm , 32 ps) is used as the pump beam and a continuum, generated by focusing part of the fundamental laser beam in a deutarated water cell, is used as the probe beam. Pump fluence at the sample is typically 5.6 mJ/cm^2. The time delay between the two beams is adjusted from 100ps to 1.5ns using a variable delay line. Time zero is defined in correspondence with pump-probe overlap. The sample is placed inside a Kerr gate composed of two perpendicular polarisers. After interaction inside the sample, the probe beam is dispersed by a spectrometer coupled to a CCD camera. The pump beam, with strong intensity,

induces transient birefringence and dichroism in the initially isotropic sample. The probe beam is initially linearly polarised at 45° to the linear polarisation of the pump beam. The induced anisotropy results in a change of the probe beam polarisation after interaction within the sample. This change is recorded for each wavelength of the continuum. Intensity measurements are averaged over 120 shots for each angle of the analyser. In particular, measurement of the dichroic angle dφ (i.e. imaginary part of the induced anisotropy) allows a direct determination of the induced dichroism (difference of absorption coefficients between two perpendicular directions). The spectral dependence of dφ is directly related to that of the absorbance, while its time dependence provides information both on the excited state relaxation dynamics and on the molecular orientational diffusion inside the solvent. The Kerr ellipsometry signal resulting from one photon excitation at 355 nm can be attributed to the excited state absorption features of the material.

For all measurements, solutions in toluene of 5 x 10^{-5} M were employed. The KE signal of 3PV, shown in Figure 8, is characterised by two main features. A photoinduced absorption (PIA) feature at 650 nm accompanies what appears to be a bleaching at 450 nm. The main absorption band does not appear until ~400nm, however, and so this increase in light flux is more likely a photoluminescent emission. The spectra recorded at longer time delays have the same profile as the one observed at zero-delay decreasing with a mono-exponential decay. This behaviour is typical of the decay of a single photogenerated molecular species with no indication of triplet or other secondary species.

Shown in Figure 9, the photoinduced absorption of HE-PmPV exhibits similar features to that of 3PV. Again, a photoinduced absorption (PIA) feature at 650 nm accompanies what is most likely a photoluminescent emission at ~450nm. However, at longer time delays, there is a deformation of the peak at 650 nm. This suggests a probable transformation of the singlet exciton state most probably to a self trapped exciton or polaronic state. Figure 10 shows the KE signal of W-PmPV. The signal is characterised by three main features. Similarly to the other materials, a "bleaching" is seen at 450 nm. The PIA feature at 650 nm is characterised by a fast decay. As it decays a new feature appears at 810 nm. Initially, this feature increases and shifts to 815 nm. After 133ps, the increase ceases and the feature decays to zero. The evolution of a secondary peak from the initial PIA peak at 650 nm is behaviour distinct from that observed in the 3PV and HE-PmPV.

As the 3PV shows simple mono-exponential decay kinetics, the PIA feature can be assigned to intra-molecular excitations where radiative decay is the dominant mechanism. Similar behaviour is observed for the HE-PmPV, although the singlet exciton is seen do evolve somewhat over the time scale of the measurement. In the case of W-PmPV, the decay feature at 650 nm coincides with the growth of a new feature at 815 nm. The exact nature of this feature is unclear. While a triplet-triplet transition cannot be discounted, it is possible that the initially excited S1 state transforms into a lower energy delocalised state across a number of chains (i.e. charge transfer exciton). In the previous section there were suggestions that W-PmPV is much more prone to aggregation than HE-PmPV even at low concentrations. It is apparent that the HE-PmPV behaves similarly to the 3PV whereas the W-PmPV shows new species attributable to aggregation.

In summary, aggregation and therefore the optical properties of PmPV-co-DOctOPV depend greatly on the isomeric character of the polymer backbone. The degree of backbone isomerism greatly effects the photoluminescence efficiency of the polymer and control over it is a route towards optimising performance.

3. Controlling Optical Properties: Multi Walled Nanotubes

Optical and IR studies clearly point towards control of backbone isomeric structure as a factor in controlling how polymer chains pack in the solid state. In this section, the use of carbon nanotubes in controlling aggregation is explored and described. Recently, a new approach to solubilise MWNT that facilitates purification and processibility was reported[23]. Through modification of a PPV structure, high wettability between PmPV-co-DOctOPV and the lattice of the nanotubes can be achieved.. It has been demonstrated for MWNT that wrapping of polymer ropes around the tube lattice occurs in a well-ordered periodic fashion[24]. The suggestion is that the polymer/toluene solutions act as a solvent for the nanotubes. The formation of these hybrid solutions has made extensive opto-electronic characterisation possible[25,26].

3.1 Materials Preparation and Characterisation

MWNT were produced using the arc discharge method[27]. It is well known that various other carbonaceous materials such as turbostratic graphite (TSG) and carbon onions accompany nanotubes produced in this manner. Hybrid solutions were

prepared by adding various MWNT loading fractions (by weight) to polymer toluene solutions.

As an example, 80 mg of HE-PmPV-co-DOctOPV were mixed with 25.5 mg of MWNT containing Krätschmer-generated carbon soot in 4 ml of toluene. The mixture was then sonicated for 4 hours in a sonic bath. The solution was allowed to stand undisturbed for 48 hours after which the sediment was removed by decantation. This sediment was then dried and weighed. It should be noted that W-PmPV was incapable of holding any material in solution.

To clarify, the natures of the sediment and remaining solute were studied using electron paramagnetic resonance (EPR)[23]. Electron paramagnetic resonance concerns the resonant absorption of microwaves in the presence of a magnetic field. For a spin half system transitions are induced between the $m_s=1/2$ and $m_s= -1/2$ spin states of any unpaired electrons in the sample. Information on the environment of the electron can be deduced from the position (described by the g value), width and shape of the absorption line. For technical reasons the first derivative of the line shape is usually reported.

EPR measurements were made at room temperature using 100 kHz field modulation, a microwave frequency of approximately 9.7 GHz and a TM011 mode cavity. To avoid distortion of the spectrum the modulation amplitude was kept at less than or equal to one third of the peak-to-peak linewidth. Calculation of g values was carried out by comparison of the signal with that of a sample with known g value for example that of F^+ centers in MgO with g=2.0023. The field range was calibrated with a proton NMR probe which gave absolute field values. Changes in signal intensity related to changes in the Q factor due to the presence of the (lossy) sample were corrected for by using the measured attenuation of the MgO F^+ signal in the presence

of the sample. For a given paramagnetic species the EPR signal intensity is proportional to the number of paramagnetic centres in the measured sample.

To prepare samples for EPR 7 mg of the separated solute were drop cast onto a spin free quartz plate. In addition the recovered sediment was carefully weighed and approximately 7 mg placed in a spin free quartz tube. Shown in Figure 11 are the EPR derivative spectra for the dispersed carbon soot and the separated sediment and solute samples. In all cases these spectra could be fitted to two Lorentzian absorption lines. In the case of the dispersed carbon soot and the sediment, g values determined from the line positions, of approximately 2.011 and 2.020 and peak-to-peak line widths, ΔB_{pp}, of close to 11 G and 12 G respectively were observed. Similar results were obtained for the solute spectra, which could be fitted to two lines with g values of approximately 2.011 and 2.020 and widths of 7 G and 18 G respectively. This demonstrates that the carbon soot consists of the same two components as are in the solutes and sediments. The variation in linewidth between sediment and solute is probably due to small environmental variations between the two phases. Two such components have been observed by other authors who attribute them to paramagnetic centers in nanotubes[28,29,] and TSG[30].

In addition to g values and linewidths, signal intensities can be measured for both the MWNT and TSG. In each case the signal intensities were normalised to represent all the unpaired spins in the total mass of sediment or solute. Using this information it is possible to calculate the percentages of both MWNT and TSG that have remained in solution. This can be calculated for a given species from

$$ \% = 100 \times \frac{NSI_{\text{solution}}}{NSI_{\text{solution}} + NSI_{\text{sediment}}} $$

Equation 2

where % is the percentage of the given species (MWNT or TSG) in solution, NSI_{solution} and NSI_{sediment} are the normalized signal intensities for the same species in solution and sediment respectively. Using this we can calculate that 63% of the added nanotubes go into solution while only 1.9% of the added TSG remains in solution.

3.2   Optical Characterisation

Figure 12a shows the fluorescence spectra of the 1×10^{-4} M solution of HE-PmPV in toluene for various mass fractions of the MWNT powder. The 0% sample (curve A) shows a well-resolved feature centred at 480 nm and a broad shoulder centred at 460nm. At this concentration, the system is already exhibiting substantial amounts of aggregation. As the nanotubes are introduced (curve B-E), the peak and the shoulder seem to resolve into two discrete features. Initially, there is also an increase in intensity of the profile. However, as the mass fraction is increased further, the intensity begins to decrease, until saturation at 9% (curve E).

The effect of nanotube introduction on the emission profile of the polymer is clearer in Figure 12b. The integrated emission as a function of polymer concentration is plotted as a solid line. As the concentration of polymer is decreased, there is a notable increase in integrated emission. This continues until 10^{-6} M is reached, at

which point the system is no longer aggregating. For the 10^{-2} M solution (point A), MWNT soot was added sequentially. The change in integrated emission with mass fraction is shown. At low mass fractions there is an initial increase. The addition of MWNT mimics a reduction in polymer concentration in the pristine system within error. This continues until 5% is reached (point D). At this point, the integrated emission begins to decrease again until it reaches a minimum at 7 % mass fraction (point E).

These effects maybe due to the nanotubes counteracting the concentration effect seen in the polymer. This "dilution effect" means that the shape and intensity of the emission profile can be controlled. At higher mass fractions, the nanotubes seem to reach a saturation concentration. Although, the shape of the profile is still fully resolved, the intensity begins to decrease. The weak broad absorption in the visible/near IR from the nanotubes may begin to play a role as they saturate the polymer matrix.

The exact nature of the interaction between the polymer backbone and the MWNT is still unclear. As stated above, when we attempted to make hybrid solutions using W-PmPV, the nanotubes do not stay in solution indicating that the interaction is dependent on backbone structure. In the next section, electron microscopy and computer simulation are used to elucidate the exact nature of the interaction in order to explain the phenomena witnessed in the optical properties and dependence on backbone isomerism.

3.3   Nature of Interaction

Computer simulation was used to identify which polymer characteristics are necessary to hold nanotubes in solution[31]. The AMPAC package was employed in all calculations[32]. Energy based simulated annealing[33] was coupled to the semi-empirical Hartree-Fock Austin Model 1 (AM1) formalism[34] to locate minima on the potential energy surface. The geometry of the lowest energy minimum was then further optimised with greater precision. Let us first examine what can be derived from experiments. It has been established that PmPV-co-DOctOPV with high *trans*/*cis* vinylene connection ratio is necessary to hold nanotubes in solution. PmPV-M1 (denoting PmPV-co-DOctOPV in which one octyloxy group replaced by methoxy group per repeat unit) dissolves in toluene but does not hold nanotubes in solution. PmPV-co-DOctOPV with both octyloxy groups replaced by methoxy groups does not even dissolve in toluene. Thus, the octyloxy groups play a crucial role in holding nanotubes in toluene. PS and PMMA both dissolves in toluene and coat the nanotube, but do not hold it in solution. Both PS and PMMA are non-conjugated whereas PmPV-co-DOctOPV is π-conjugated.

The optimised geometry of 4 repeat unit PmPV-co-DOctOPV (all *trans*) polymer is shown in Figure 13A. The backbone reorganises into a relatively flat helical structure due to meta-phenylene linkage and van der Waals interactions between the octyloxy groups. These groups are projected outwards from the helical structure, as is shown in Figure 13B.

This is compared with optimised geometry of 4 repeat unit PmPV-M1 (all *trans*), see Figure 13C. The backbone remains straight and does not reorganise into a helical structure due to only one octyloxy group. The polymer does not expose the conjugated backbone because the octyloxy groups are projected outwards under a 45-degree angle.

Thus the backbone has to be exposed in order to facilitate binding between polymer and nanotube. It is for this reason that PmPV-co-DOctOPV with two octyloxy groups can hold nanotubes in solution, whereas PmPV-M1 (with one octyloxy group) is not able to do this. Figure 14A and B show the optimised geometry of all *cis* PmPV-co-DOctOPV. The backbone reorganises into a non-exposed non-regular helical structure with solubilising sidegroups pointing upwards and outwards. As a result of its non-regular backbone, the all *cis* polymer coats the nanotubes through van der Waals forces. However, this interaction is not strong enough to hold the nanotubes in solution. Moreover, the all *cis* configuration could facilitate entanglements between polymer sidegroups, resulting in formation of aggregates, which inhibit nanotube coating. Molecular dynamics simulations of these polymers in toluene at room temperature confirm the optimised geometries of Figures 13 and 14[35]. This may explain why the predominantly cis-polymer shows signs of aggregation at much lower concentrations than the predominantly trans-polymer.

Combining experimental evidence and computer simulation we propose the following explanation for successful interaction between polymer and nanotube, necessary to hold nanotubes in solution. It was found that all *trans* PmPV-co-DOctOPV successfully holds nanotubes in solution due a flat helical backbone that facilitates electronic interaction of its π-conjugated system with the highly delocalised nanotube, in addition to weaker van der Waals interaction. Thus the polymer has to interact with the nanotube through van der Waals and electronic forces. However, this electronic interaction does not involve charge transfer, since the polymer can be removed from the nanotubes non-destructively.

The Transmission Electron Microscope (TEM) used was a Hitachi H7000, operating at an accelerating voltage of 100keV. The samples were prepared on a substrate of formvar coated copper TEM grids. These were prepared by briefly dipping the TEM grids into the composite solution and allowing to dry slowly in air. The nanotubes protruding where the polymer film had receded as the solvent evaporated were examined.

Shown in Figure 15 is an open tube partly embedded in the polymer. The polymer coating the nanotube can be clearly seen. In this instance, wrapping by the polymer occurs in a well-ordered periodic fashion. This suggests that there is correlation between the arrangement of aromatic hexagons in the nanotube's lattice structure and the surrounding polymer coating. We suggest that there could be Van der Waals interaction, analogous to J-aggregate stacking of aromatic π-systems between the benzene rings of the polymer and the hexagonal lattice structure of the nanotubes. Considering the regular spacing of the spiral structure, and the helix dimensions, we believe that polymer strands may be coiling around each other to form ropes, which in turn surround the nanotubes in a regular, structured way.

4. Conclusions

In summary, it has been shown that the conformation and hence the optical properties of poly(*m*-phenylenevinylene-co-2,5,-dioctyloxy-*p*-phenylenevinylene) varies greatly with concentration in solution. We have proposed two methods in which to control these effects. The polymer has been prepared in a predominantly *cis* and a predominantly *trans* configuration respectively. The optical studies indicate that the *cis*-polymer is prone to inter-chain interaction at much lower concentrations than

the *trans*-polymer. The results point to the importance of backbone configuration in determining the optical properties of the polymers. This morphology and hence aggregation, can be controlled to some extent by the synthetic route. To this end the polymer has been prepared at various temperature to precisely control the isomeric character of the backbone[36]   However, interactions between chains are a determining factor in the optical properties and control of them remains a priority.

Another method to inhibit inter-chain interaction is the incorporation of multi wall nanotubes into the polymer solution. Spectroscopic studies of multi walled nanotube- polymer hybrids have been carried out. We have shown that there is a weak interaction between the polymer backbone and the nanotubes. At low mass fractions, the nanotubes act to prevent aggregation in the polymer system and the polymer-tube interaction most likely accounts for modifications to the emission spectrum. Electron microscopy indicates that the nanotube in solution have a uniform coating of polymer. This coating is structured and periodic, implying a correlation between the coating and the nanotube beneath. These facts show that these constituents are not only miscible but are actually bound to each other in a well-organised and controlled way. When the coiling of polymer strands is more disordered the interaction between the two species is highly impaired and the nanotubes are no longer able to stay in solution. This was the case when nanotubes were introduced into a *cis*-rich polymer where the coiling is non-regular.

References

[1] N.C. Greenham, R.H. Friend, Solid State Phys. 49 (1995) 1

[2] J.H. Burroughs, D.D.C. Bradley, A.R. Brown, R.N. Marks, K. Mackay, R.H. Friend, P.L. Burn, A.B. Holmes, Nature 347 (1990) 539

[3] J.C. Carter, I. Grizzi, S.K. Heeks, D.J. Lacey, S.G. Latham, P.G. May, O.R. De los Panos, K. Pichler, C.R. Towns, H.F. Wittman, App. Phys. Lett. 71 (1997) 34

[4] J. Salbeck, Ber. Bunsen-Ges. Phys. Chem. 100 (1996) 1667

[5] Y. Pang, J. Li, B. Hu, F.E. Karasz, Macromolecules 32 (1999) 3946

[6] B. Xu, J. Zhang, Y. Pan, Z. Peng, Synth. Met. 107 (1999) 47

[7] C.L. Gettenger, A.J. Heeger, J.M. Drake, D.J. Pine, J. Chem. Phys. 101 (1994) 1673

[8] L. Chiavarone, M. Di Terlizzi, G. Scamarcio, App. Phys. Lett. 75 (1999) 2053

[9] T.Q. Nguyen, R.C. Kwong, M.E. Thompson, B.J. Schwartz, App. Phys. Lett. 76: (2000) 2454

[10] S. Son, A. Dodabalapur, A.J. Lovinger, M.E. Galvin, Science 269 (1995) 376

[11] F. Cacialli, R. Daik, W. J. Feast, R.H. Friend, C. Lartigau, Opt. Mat. 12 (1999) 315

[12] B. Hu, Z. Yang, F.E. Karasz, J. App. Phys. 76 (1994) 2419

[13] W. Holzer, A. Penzkofer, S.H. Gong, A. Bleyer, D.D.C. Bradley, Adv. Mat. 9 (1999) 974

[14] D.F. O'Brien, A. Bleyer, D.D.C. Bradley, T. Tsutsui, J. Appl. Phys. 82 (1997) 2662

[15] H. Meier, Angewandte Chemie 31 (1992) 1399

[16] R. Saito , G. Dresselhaus , M. S. Dresselhaus , Physical Properties of Carbon Nanotubes, Imperial College Press, London, 1998.

[17] M. S. Dresselhaus, G. Dresselhaus, P. C. Eklund, Science of Fullerenes and Carbon Nanotubes, Academic Press, San Diego, CA 1999.

[18] A.P. Davey, A. Drury, S. Maier, H.J. Byrne, W.J. Blau, Synth. Met. 103: (1999) 2478

[19] D. Bradley, Thesis, Dublin Institute of Technology, 2000

[20] T.-Q. Nguyen, V. Doan, B.J. Schwartz J. Chem. Phys. 110 (1999) 4069

[21] I.D.W. Samuel, G. Rumbles, C.J. Collison, R.H. Friend, S.C. Moratti, A.B. Holmes, Synth. Met. 84 (1997) 995

[22] N. Pfeiffer, F. Charra, J.-M. Nunzi, Opt. Lett. 16 (1991) 1987

[23] J. N. Coleman, A. B. Dalton, S. Curran, A. Rubio, A. P. Davey, A. Drury, B. McCarthy, B. Lahr, P. M. Ajayan P, S. Roth, R. C. Barklie, W. J. Blau W, Adv. Mater. 12 (1999) 213

[24] B. McCarthy, J. N. Coleman, S. Curran, A. B. Dalton, A. P. Davey, Z. Konya, A. Fonseca, J. B. Nagy, W. J. Blau, J. Mat. Sci. Lett. In Press

[25] B. McCarthy, J. N. Coleman, S. Curran, A. B. Dalton, A. P. Davey, Z. Konya, A. Fonseca, J. B. Nagy, W. J. Blau, J. Mat. Sci. Lett. In Press

[26] S. A. Curran, P. M. Ajayan, W. J. Blau, D. L. Carroll, J. N. Coleman, A. B. Dalton, A. P. Davey, A. Drury, B. McCarthy, S. Maier, A. Strevens, Adv. Mater. 10 (1998) 1091.

[27] W. Kraetchmer, L.D. Lamb, K. Fostiropoulos, D.R. Huffman, Nature 347 (1990) 354

[28] O. Chauvet, L. Forro, W. Bacsa, D. Ugarte, B. Doudin, W. A. de Heer, Phys. Rev. B. 52 (1995) 6963

[29] S. Bandow, J. Appl. Phys. 80 (1996) 1029

[30] H. Araki, R. Matsuoka, K. Yoshino, M. Fukuda, S. Mizogami, J. Appl. Phys. 69 (1991) 7244

[31] M. in het Panhuis, R.W. Munn, W.J. Blau, accepted for publication in Synthetic Metals.

[32] Ampac 6.0, 1997, Semichem, 7128 Summit, Shawnee, KS 66216, U.S.A.

[33] F. Bockisch, D. Liotard, J.C. Rayez, B. Duguay, Int. J. Quant. Chem. 44 (1992) 619.

[34] M.J.S. Dewar, E.G. Zoebisch, E.F. Healy,J.J.P. Stewart, J. Am. Chem. Soc. 107 (1985) 3902.

[35] M. in het Panhuis, J.N. Coleman, W.J. Briels and W.J. Blau, to be published.

[36] A. Drury et al, to be published.

Figure Captions

Figure 1:

Nominal chemical structure of poly(*m*-phenylenevinylene-co-2,5-dioctyloxy-*p*-phenylenevinylene) (PmPV-co-DOctOPV).

Figure 2:

Absorption and Luminescence spectra of polymer solutions in Toluene: HE-PmPV (A) and W-PmPV (B) at a concentration of 5×10^{-5} M in 1mm cuvettes.

Figure 3:

Normalised absorption spectra, as a function of concentration, for HE-PmPV.

Figure 4:

Luminescence spectra, as a function of concentration, for HE-PmPV.

Figure 5:

Normalised absorption spectra, as a function of concentration, for W-PmPV.

Figure 6:

Photoluminescence spectra, as a function of concentration, for W-PmPV

Figure 7:

Infra-red spectra for both HE-PmPV (A) and W-PmPV (B). Features indicative of CH wag for *cis* and *trans* vinylene bonds are labelled.

Figure 8:

Dichroic spectra of 3PV in solution with toluene. The spectra are recorded at 0, 133ps and 266ps time delay after 355nm excitation. Base line is shifted upward for clarity.

Figure 9:

Dichroic spectra of HE-PmPV in solution with toluene. The reported spectra are recorded at 0, 66ps and 199ps time delay after 355nm excitation. Base line is shifted upward for clarity.

Figure 10:

Dichroic spectra of W-PmPV in solution with toluene. The reported spectra are recorded at 0, 133ps and 199ps time delay after 355nm excitation. Base line is shifted upward for clarity.

Figure 11:

EPR derivative spectra for some of the samples studied in this work. EPR spectra of A) Carbon soot dispersed in toluene, B) the sediment formed after 48 hours settling time and C) the solute remaining after 48 hours settling time. Note that in spectra A and B two components, representing nanotubes and impurities, are clearly present. In the case of spectrum C the sole component present is that of the nanotubes

Figure 12:

A) Photoluminescence spectra of HE-PmPV/MWNT hybrid solutions for various mass fraction MWNT loading. Initial polymer concentration is 1×10^{-4} M. MWNT loading fractions are (a) 0%, (b) 3%, (c) 5%, (d) 7%, (e) 9%

B) Solid Line: Integrated photoluminescence intensity as a function of concentration in toluene solution. Spots: Integrated photoluminescence intensity as a function of MWNT loading fraction added to 1×10^{-2} M solution of HE-PmPV in toluene.

Figure 13:

Computer simulated energy minimised structures of all *trans* PmPV-co-DOctOPV. A) top and B) side view. C) side view of all *trans* PmPV-M1. Carbon, hydrogen and oxygen atoms are shown in grey, white and red respectively.

Figure 14:

Computer simulated energy minimised structures of all *cis* PmPV-co-DOctOPV. A) top and B) side view. Carbon, hydrogen and oxygen atoms are shown in grey, white and red respectively.

Figure 15:

An open tube coated in polymer. Note the periodicity of the wrapping along the nanotube body. Scale bar denotes 100 nm. Inset shows a close up of the wrapping process. Diameter of nanotube shown is approx. 25 nm. Arrows highlight some of the repeating helical structure.

Figure 1

Figure 2

A: 1×10^{-6} M
B: 5×10^{-6} M
C: 1×10^{-5} M
D: 5×10^{-5} M
E: 5×10^{-4} M
F: 1×10^{-3} M

Figure 3

A: 1 x 10^{-5} M
B: 5 x 10^{-5} M
C: 5 x 10^{-4} M
D: 1 x 10^{-3} M
E: 5 x 10^{-3} M

Figure 4

Figure 5

A: 1 x 10^{-5} M
B: 5 x 10^{-5} M
C: 1 x 10^{-4} M
D: 5 x 10^{-4} M
E: 1 x 10^{-3} M
F: 5 x 10^{-3} M
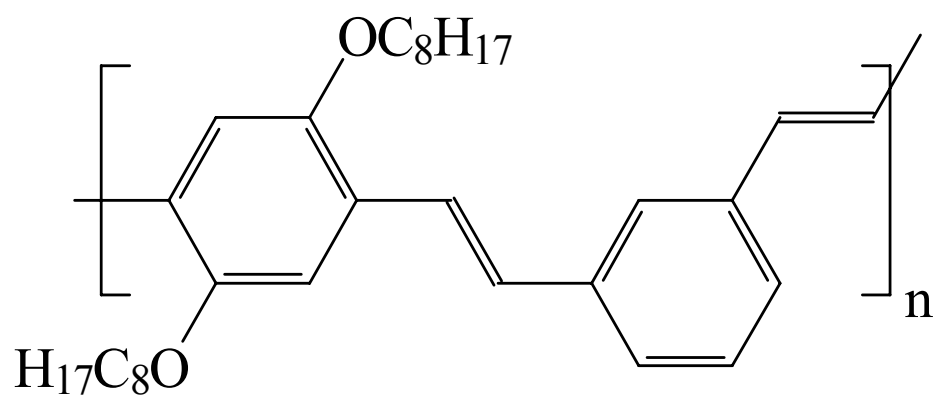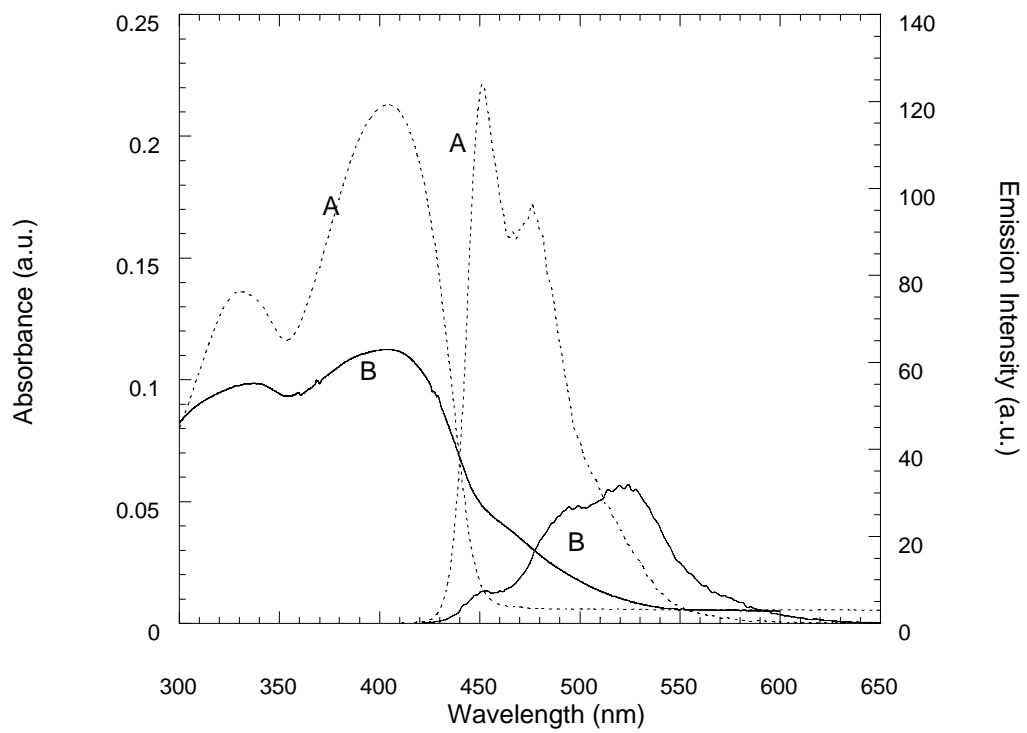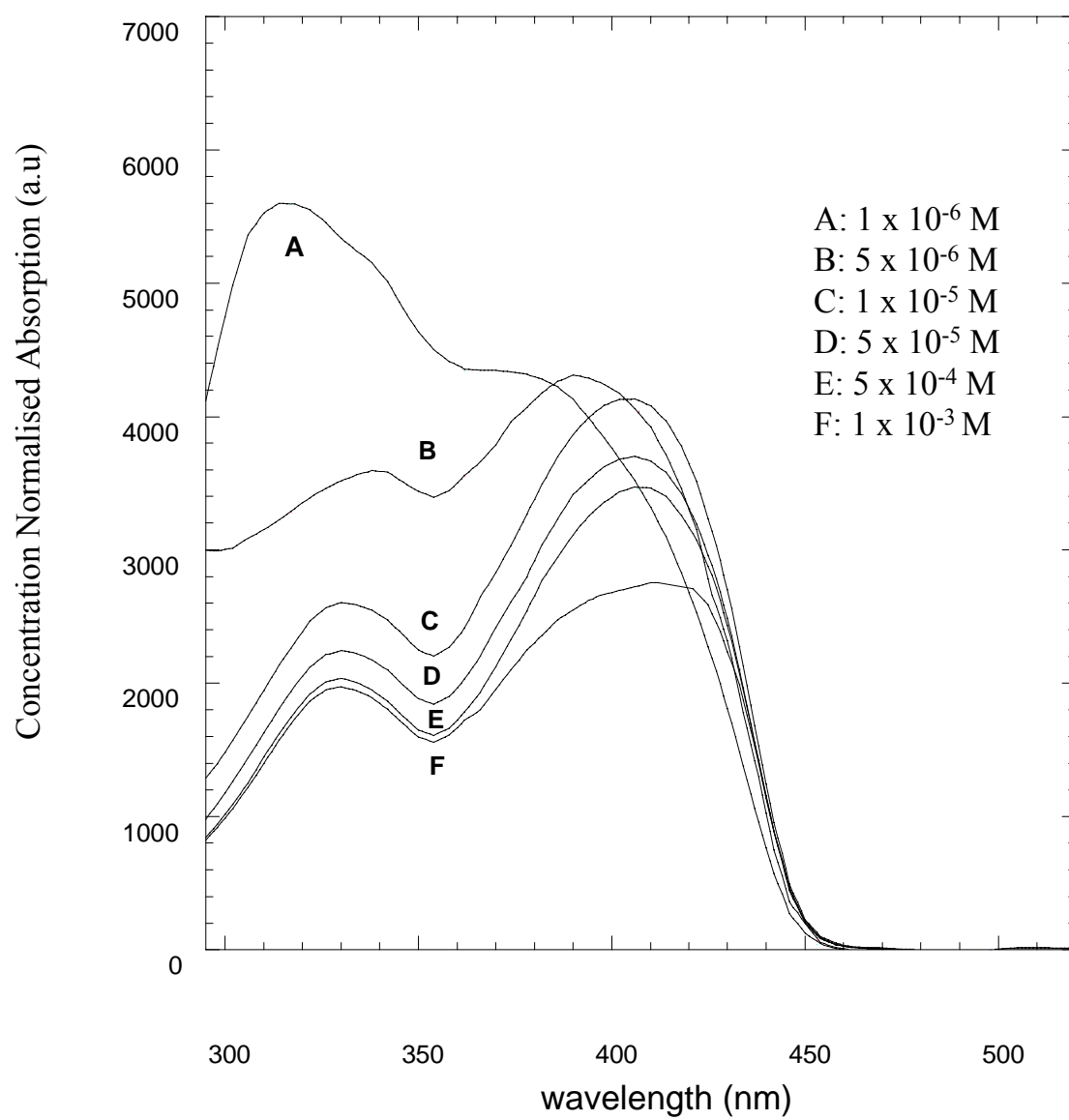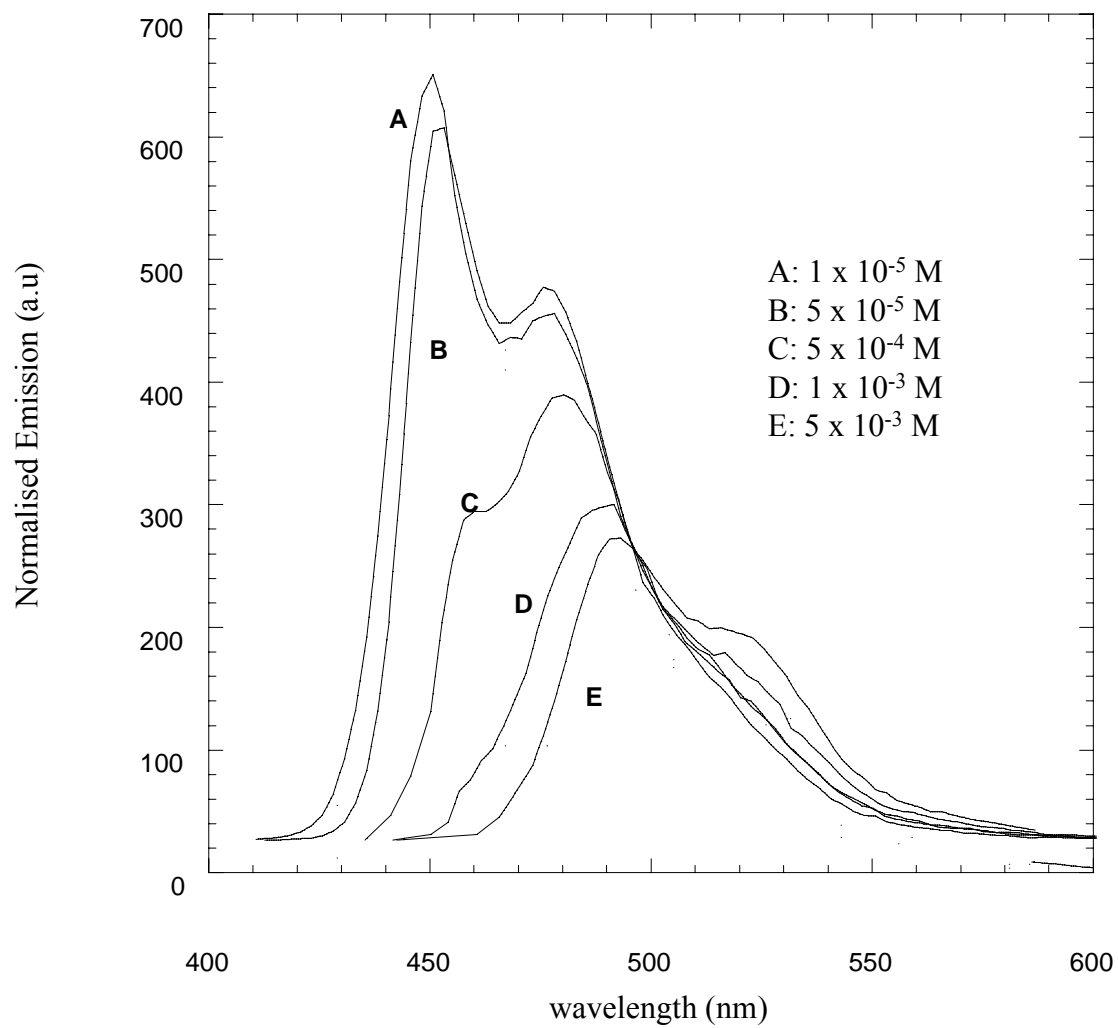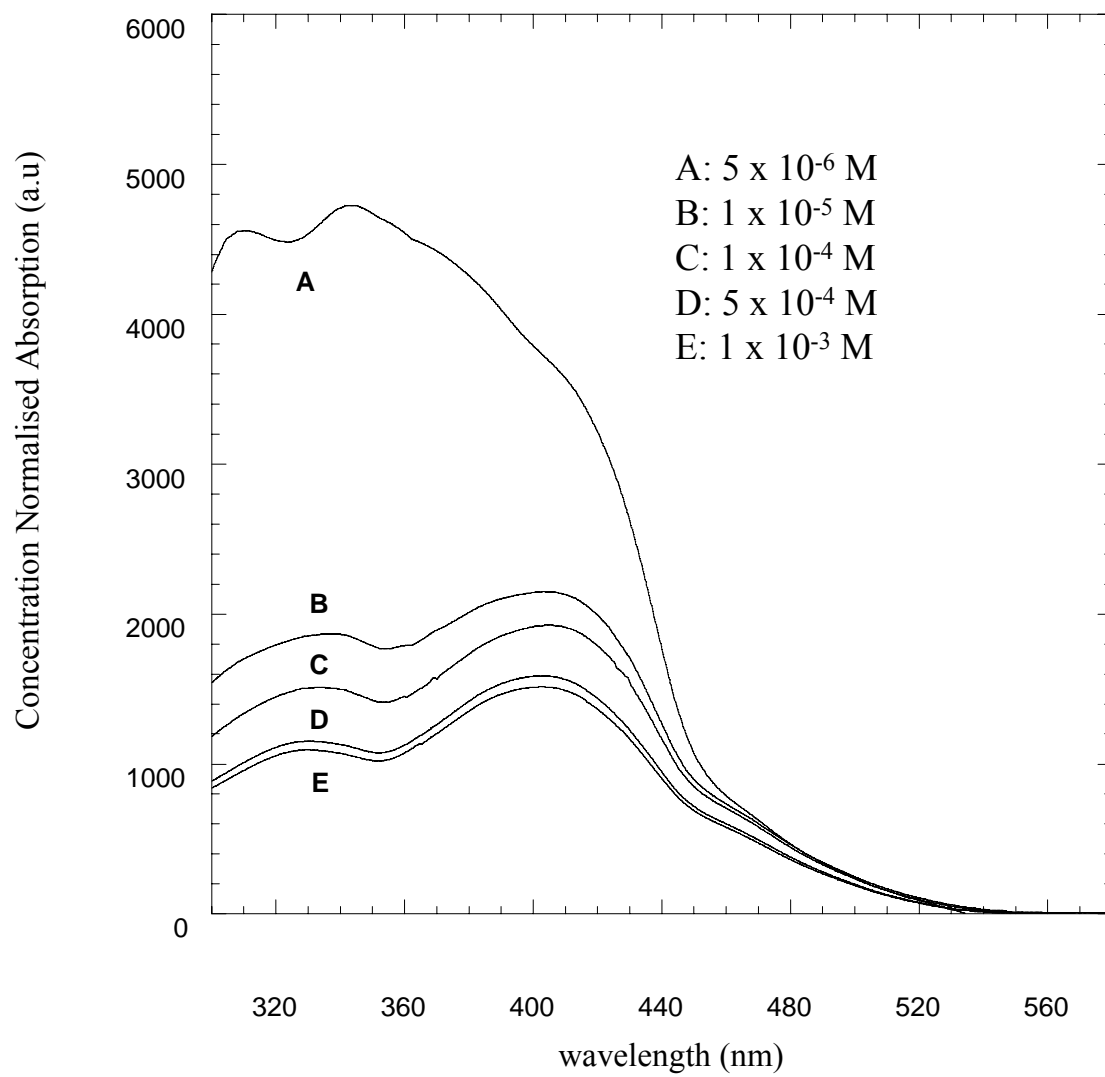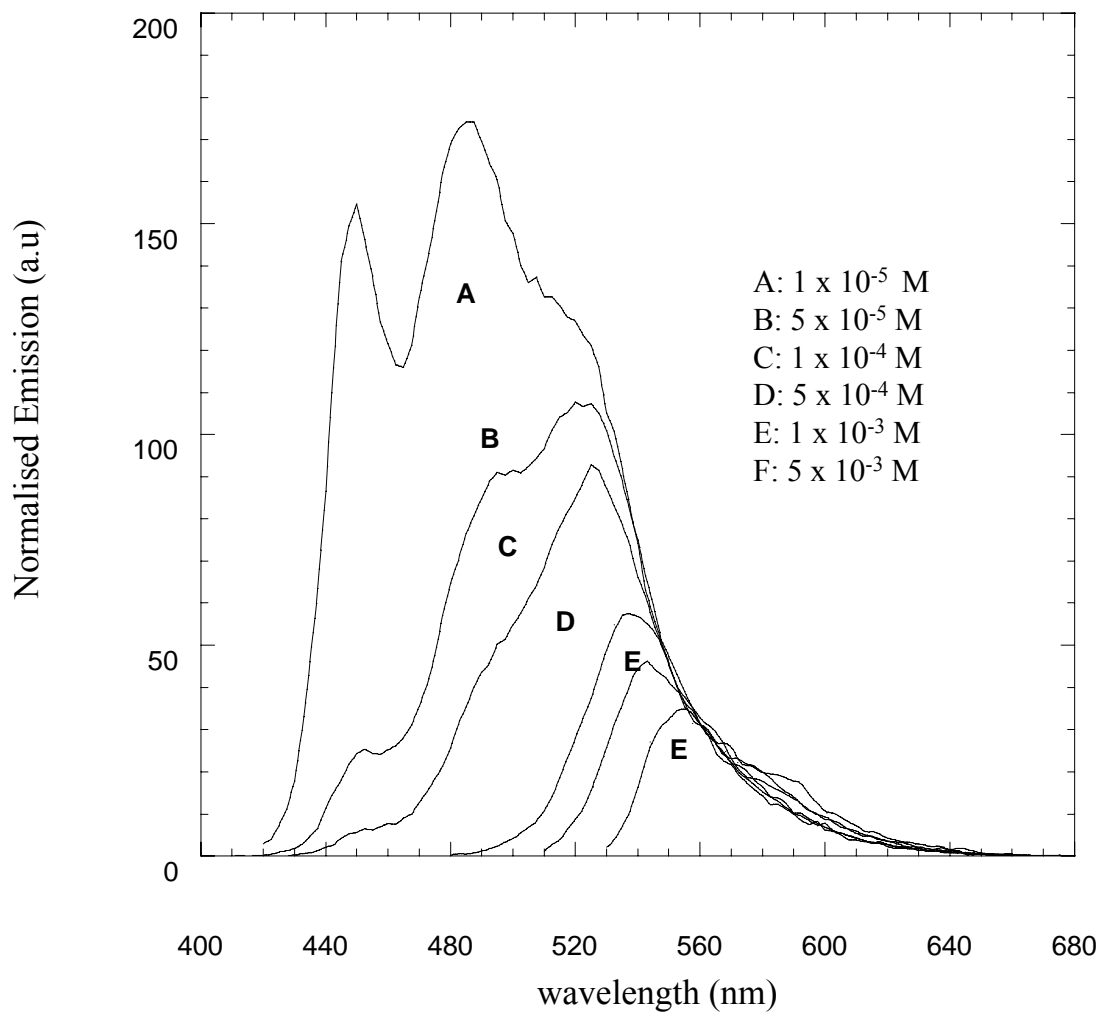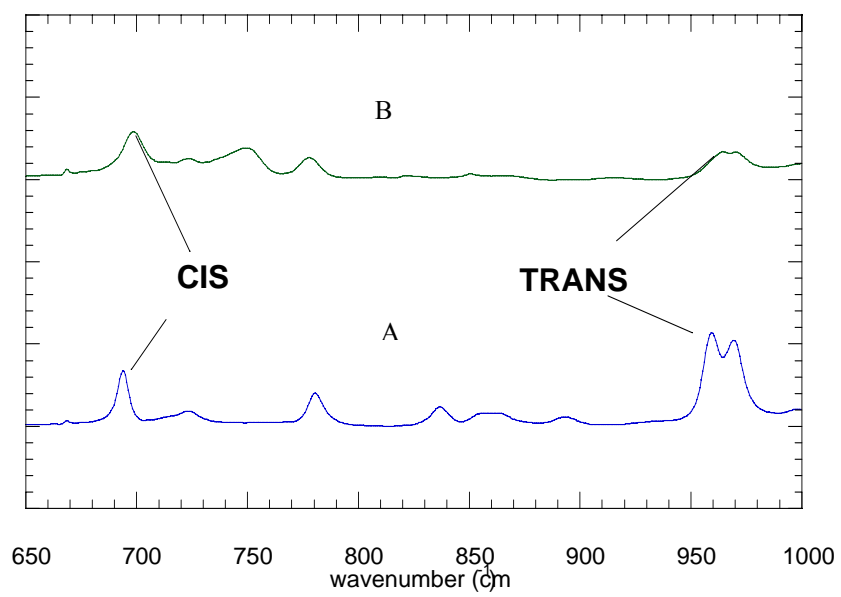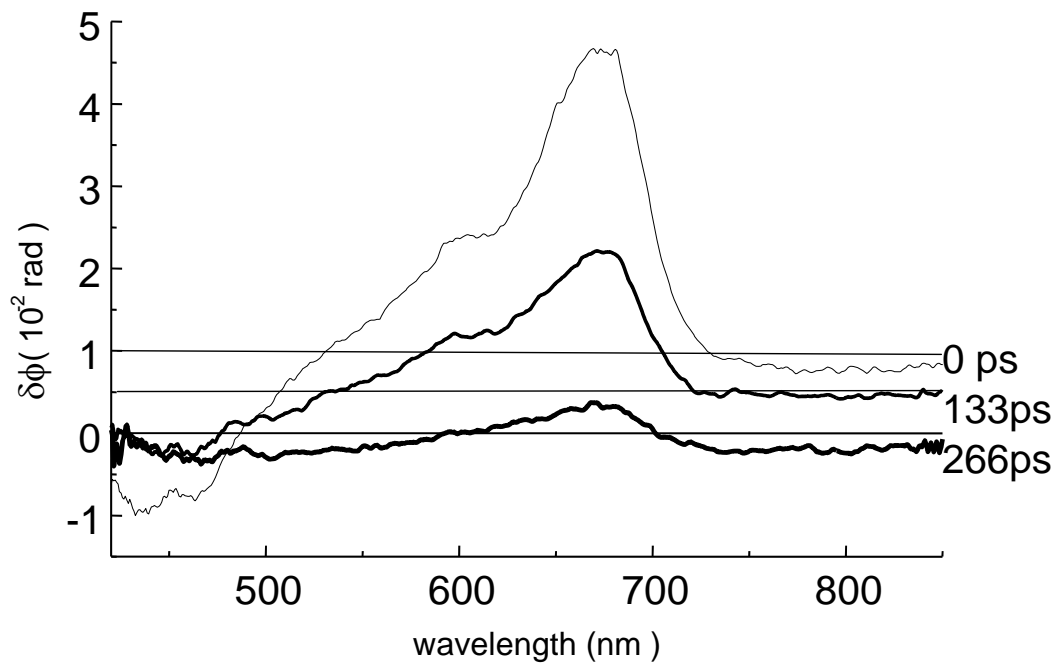
Figure 6

Figure 7

Figure 8
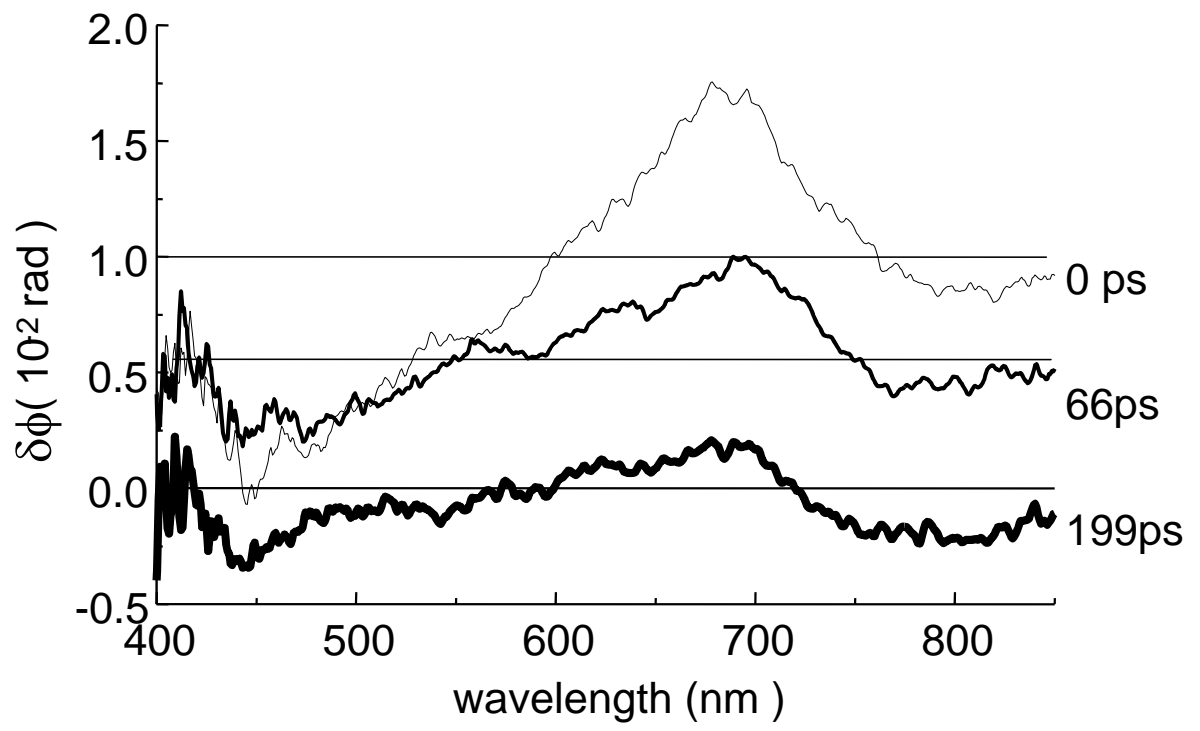
Figure 9
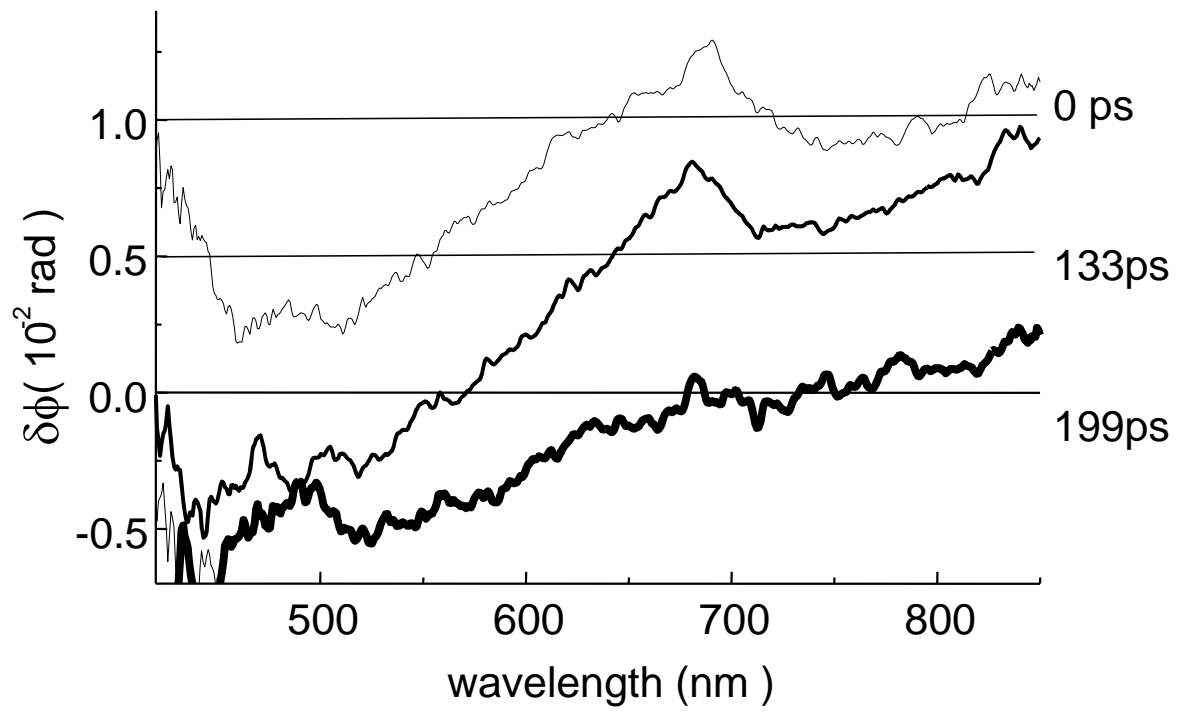
Figure 10

3300   3400   3500
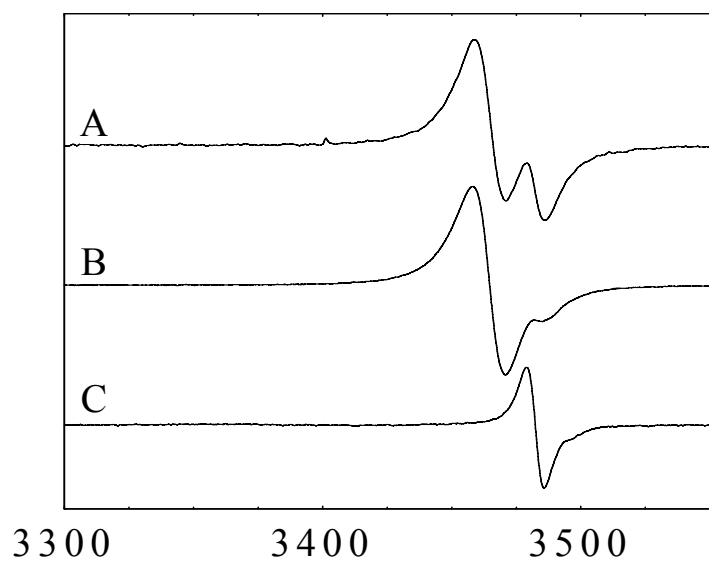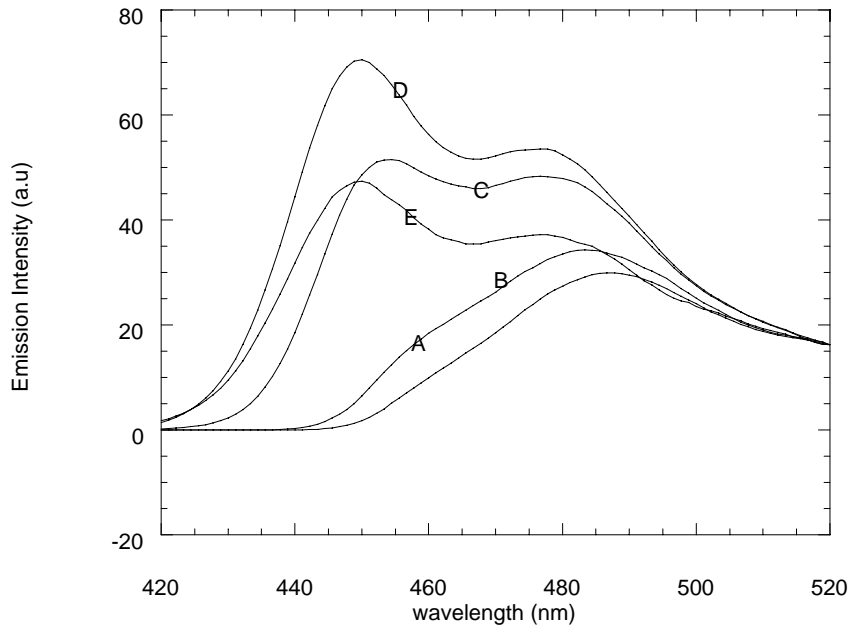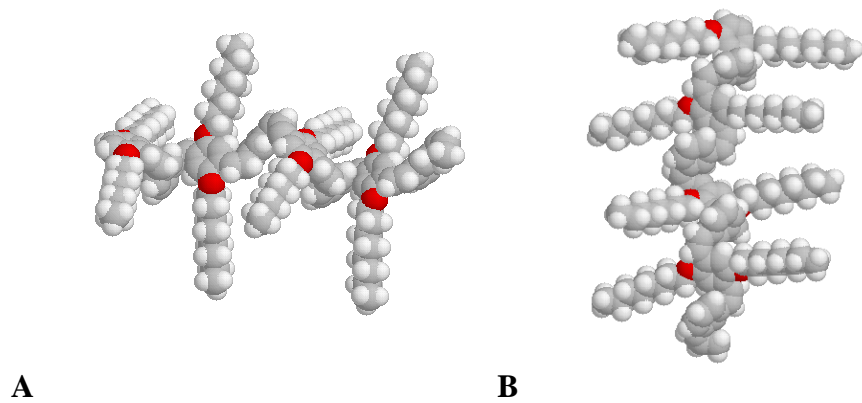
Figure 11

Figure 12 a

Figure 12 b

Figure 12

A   B

C

Figure 13

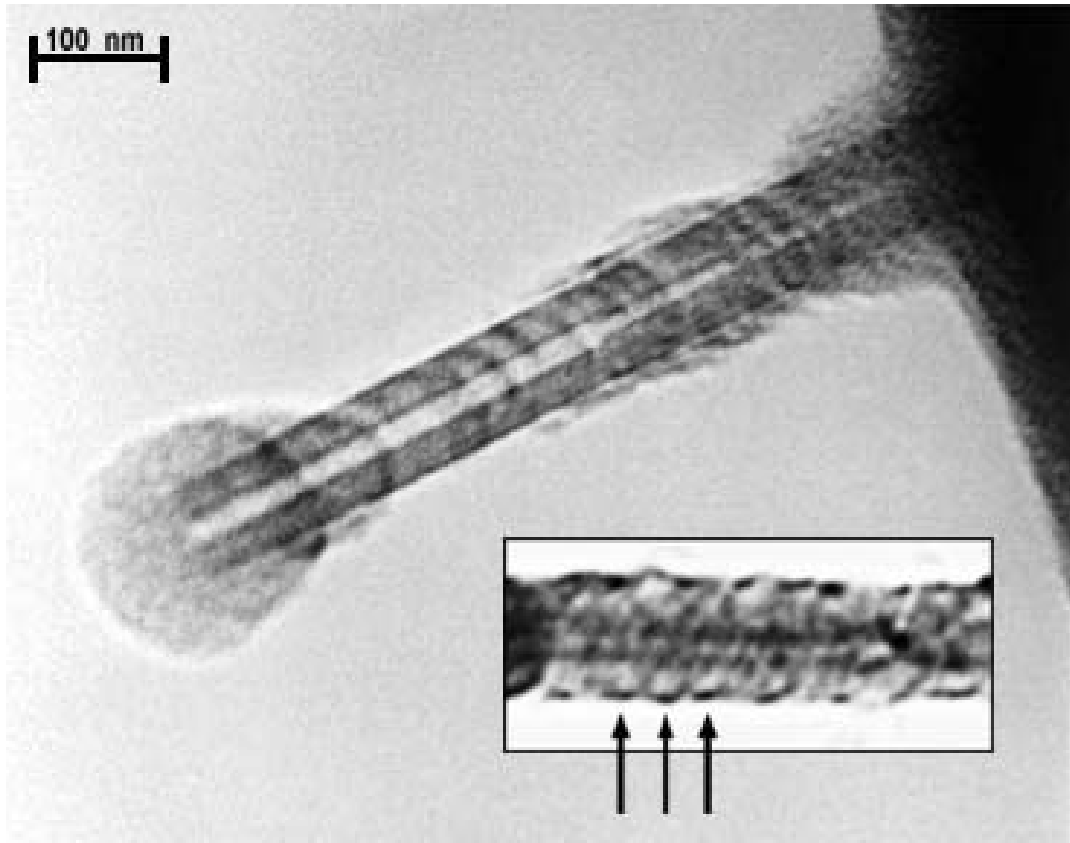

A   **B**

Figure 14

41

Figure 15